

Elasticity-driven Nanoscale Texturing in Complex Electronic Materials

A.R. BISHOP¹ T. LOOKMAN¹, A. SAXENA¹ and S.R. SHENOY²

¹ *Theoretical Division, Los Alamos National Laboratory, Los Alamos, NM, 87544 USA*

² *International Centre for Theoretical Physics, Trieste 34014, Italy*

PACS. 71.38.-k - .

PACS. 75.47.Gk - .

PACS. 74.72.-h - .

Abstract. – Finescale probes of many complex electronic materials have revealed a non-uniform nanoworld of sign-varying textures in strain, charge and magnetization, forming meandering ribbons, stripe segments or droplets. We introduce and simulate a Ginzburg-Landau model for a structural transition, with strains coupling to charge and magnetization. Charge doping acts as a local stress that deforms surrounding unit cells without generating defects. This seemingly innocuous constraint of elastic ‘compatibility’, in fact induces crucial anisotropic long-range forces of unit-cell discrete symmetry, that interweave opposite-sign competing strains to produce polaronic elasto-magnetic textures in the composite variables. Simulations with random local doping below the solid-solid transformation temperature reveal rich multiscale texturing from induced elastic fields: nanoscale phase separation, mesoscale intrinsic inhomogeneities, textural cross-coupling to external stress and magnetic field, and temperature-dependent percolation. We describe how this composite textured polaron concept can be valuable for doped manganites, cuprates and other complex electronic materials.

High resolution microscopies of many classes of complex electronic materials such as cuprates, manganites, ferroelastic martensites, and relaxor ferroelectric titanates [1, 2, 3, 4] have revealed previously unsuspected, and puzzling, multiscale modulations of charge, spin, polarization and strain variables in stripe- or droplet-like patterning over 1-100 nm scales, or up to hundreds of lattice spacings. These sign-varying inhomogeneities or ‘texturings’ fundamentally affect *local* electronic, magnetic and structural properties, and appear to be *intrinsic*: arising from the coupling between degrees-of-freedom, rather than induced by extrinsic disorder.

Ferroelastic martensitic alloys like FePd, and the more complex cuprates and manganites, typically have displacive first-order structural transitions [1], described by *symmetry-adapted* strain tensor components as order-parameters (OP), with 1-10 nm criss-cross ‘tweed’ strain variations above, and 10-100 nm ‘twins’ below, the structural transition [1]. There is evidence for lattice/charge/spin coupling in both cuprates and manganites in: isotope effects [5]; doping-dependence of transition temperatures [1]; polaron signatures with [4] temperature- and field-dependent four-lobe signatures in diffuse X-ray and neutron scattering;

field-dependent wandering ribbons of high conductivity [1, 2, 6] ; and (fluctuating or static) stripe bubbles of modulated buckling-angle and spin [3]. A strain-magnetization coupling is indicated by *cross*-responses [7]: e.g., manganites that show colossal magneto-resistance (CMR) in magnetic fields also show colossal ‘stress-resistance’ (CSR) under hydrostatic pressure.

The central questions are conceptual: what excitations result, when doped local charges in a (para- or antiferro-) magnetic background couple to a nonlinear elastic lattice that supports a structural transition? What is the origin of multiscale intrinsic inhomogeneities?

We adopt a Ginzburg-Landau (GL) approach, with three generic model assumptions: (1) The free energy is harmonic in the non-order-parameter strain components and nonlinear in the order-parameter strain (with multiple wells just above, and below, structural transition temperatures); (2) The charge density and magnetization variables couple locally, in symmetry-allowed ways, to different symmetry-adapted strain-tensor components, (and can then act like local internal stresses or temperatures); (3) The charge carriers deforming a unit-cell do not damage the lattice by generating defects such as dislocations or vacancies (so there is a smoothly compatible matching to the farther, and decreasingly-strained, unit-cells). Long-range *isotropic* Coulomb potentials, with or without, or with electron-phonon coupling, have been invoked to explain nanoscale charged stripe patterns [8]. However, our central point here is that charges and spins locally coupled to strains of a nonlinear lattice, can induce multiscale mutual texturings through *anisotropic long-range* strain-strain forces (themselves Coulombic at a chemical-bond level [9]), that arise from generic *elastic compatibility* constraints [10].

GL model: 1. *Strain Free Energy:* We consider a two-dimensional (2D) first-order square-to-rectangular transformation as a surrogate for 3D tetragonal-orthorhombic [1] structural transitions; extensions to 3D are possible [11]. The Cauchy strain tensor \underline{E} linear in the displacement \vec{u} , is $E_{\mu\nu} = (1/2)(\Delta_\mu u_\nu + \Delta_\nu u_\mu)$, where Δ_μ is a discrete derivative in the $\mu = x, y$ directions, and small ‘geometric’ nonlinearities are ignored. The symmetry-adapted strains are the ‘rectangular’ or deviatoric $\varepsilon \equiv (1/\sqrt{2})(E_{xx} - E_{yy})$, compressional $e_1 = (1/\sqrt{2})(E_{xx} + E_{yy})$, and shear $e_2 = E_{xy}$, strains, respectively. The invariant free energy is

$$F = F^{(1)}(\varepsilon, e_1, e_2) + F^{(2)}(m) + F^{(coupling)}(n, m, \varepsilon, e_1), \quad (1)$$

with all quantities scaled [11] to be dimensionless. The strain contribution is

$F^{(1)} = (a_0/2) \sum_{\vec{r}} (\vec{\Delta} \varepsilon)^2 + F_0(\varepsilon) + F_{cs}(e_1, e_2)$, where $\sqrt{a_0}$ is a strain variation length. The Landau term is sixth-order in the deviatoric OP strain $F_0 = (\tau - 1)\varepsilon^2 + \varepsilon^2(\varepsilon^2 - 1)^2$. Here $\tau(T) = (T - T_{sc})/(T_s - T_{sc})$ is a scaled temperature, and for $4/3 > \tau > 0$, F_0 has triple wells that become degenerate at $\tau(T = T_s) = 1$, reducing to double wells for $T < T_{sc}$ or ($\tau < 0$). The compression/shear (*cs*) terms are harmonic, $F_{cs} = \sum_{\vec{r}} \frac{1}{2} A_1 e_1^2(\vec{r}) + \frac{1}{2} A_2 e_2^2(\vec{r})$.

2. *Charge and Magnetization Free Energy:* The free energy for a magnetization variable $m(\vec{r})$ is $F^{(2)}(m) = \sum_{\vec{r}} f[(\frac{am}{2})(\vec{\Delta} m(\vec{r}))^2 + (T - T_{cm})m^2(\vec{r}) + \frac{1}{2}m^4(\vec{r})] - hm$. Here f is a magnetic/elastic energy ratio, h ($\sqrt{a_m}$) is a magnetic field (length), and the zero-doping magnetic transition temperature $T_{cm} < T_s$. The symmetry-allowed couplings are

$$F^{(coupling)}(n, m, \varepsilon, e_1) = \sum_r A_{n\varepsilon} n \varepsilon^2 + A_{nm} n m^2 + [A_{n1} n e_1 + A_{m1} m^2 e_1 + p_1(\vec{r}) e_1], \quad (2)$$

where $p_1(\vec{r}) > 0$ is an external compressional stress. The $A_{n\varepsilon} n \varepsilon^2$ term is like a local temperature $\sim \tau \varepsilon^2$, and for $A_{n\varepsilon} > 0$, the charge favours the high-temperature $\varepsilon = 0$ unit-cell symmetry. The $A_{m1} m^2 e_1$ term acts like a local stress ($\sim m^2$) for e_1 , and like a local temperature ($\sim e_1$) for m^2 . We choose $A_{m1} > 0$, favouring m^2 when spins are closer ($e_1 < 0$). The m^2 coefficient in F defines an effective local temperature deviation $\tau_{cm}(T, \vec{r}) \equiv f[T - T_{cm}^{eff}(\vec{r})]/A_{m1} \equiv e_1 + [f(T - T_{cm}) + A_{nm} n]/A_{m1} \equiv \delta e_1(T, \vec{r})$. This implies a temperature-dependent percolation:

on warming, the compressed $m \neq 0$ regions below transition ($\tau_{cm}(T, \vec{r}) = \delta e_1(T, \vec{r}) < 0$) will shrink. We now *mimic* manganites and cuprates by further model choices of parameter signs and interpretations of variables.

(i) For ‘manganites’, with a zero-doping nonferromagnetic $T_{cm} = 0$ parent compound, we focus for simplicity on the magnetization-inducing *mobile* electrons produced by doping, of concentration $x_e = \langle n \rangle$ where the number density $n(\vec{r}) = \sum_i (\kappa^2/2\pi) e^{-\kappa|\vec{r}-\vec{r}_i|}$ is a sum over normalized single-charge profiles at sites i , with $2/\kappa$ the intersite tunneling length. Here the $A_{nm}nm^2$ term with $A_{nm} < 0$ means that mobile electrons lock onto and align the ferromagnetic $m(\vec{r})$ core spins (mimicking a double exchange/ Hund’s rule, term). The mobile electrons can induce an effective local [6] Curie temperature, $T_{cm}^{eff}(\vec{r}) = (-A_{nm}n - A_{m1}e_1)/f > 0$. Since metallicity shrinks unit-cell volume, we take the $A_{n1}ne_1$ term with $A_{n1} > 0$: $n(\vec{r})$ favours compression, $e_1 < 0$.

(ii) For ‘cuprates’, $n(\vec{r})$ is the local *hole* number density of doping fraction $x_h = \langle n \rangle$ into an antiferromagnetic parent compound with Néel temperature $T_{cm} \neq 0$. With $A_{nm} > 0$ in $A_{nm}nm^2$, the *staggered* magnetization $m(\vec{r})$ is reduced by hole doping. As the structural transition temperature also decreases rapidly with doping [1], we take $A_{n\epsilon} \gg 1$. Since holes repel lattice ions, the $A_{n1}ne_1$ term has $A_{n1} < 0$: $n(\vec{r})$ favours expansion, $e_1 > 0$.

3. *Elastic Compatibility and Anisotropic Long-range Potentials*: The St. Venant’s compatibility condition [10] expresses the no-defect constraint as $\vec{\Delta} \times (\vec{\Delta} \times \underline{E})^\dagger = 0$. (This is analogous to a $\vec{\Delta} \cdot \vec{B} = 0$ no-monopole condition in electromagnetism.) In 2D we have [12] $\vec{\Delta}^2 e_1 - \sqrt{8}\Delta_x \Delta_y e_2 = (\Delta_x^2 - \Delta_y^2)\epsilon$, linking OP and non-OP strains. Minimizing the free energy F_{cs} with respect to $e_{1,2}$ while maintaining the compatibility constraint, we find $e_{1,2}(\vec{k}) = B_{1,2}(\vec{k})\epsilon(\vec{k})$, where $B_1(\vec{k}) = [k_x^2 - k_y^2]k^2/[k^4 + (8A_1/A_2)(k_x k_y)^2]$ and $B_2(\vec{k}) = -(A_1/A_2)[\sqrt{8}k_x k_y/k^2]B_1(\vec{k})$. Substituting back, the seemingly innocuous harmonic F_{cs} yields [11, 12] the crucial ALR potential, encoding unit-cell fourfold symmetries,

$$F_{cs} = (A_1/2) \sum_{\vec{k}} U(\hat{k}) |\epsilon(\vec{k})|^2; \quad U(\hat{k}) = [(k_x^2 - k_y^2)^2 / [k^4 + (8A_1/A_2)(k_x k_y)^2]], \quad (3)$$

while (2) yields nonlocal couplings to the OP. Here $U(\hat{k})$ depends on the direction \hat{k} and clearly favors $\hat{k}_x = \hat{k}_y$ diagonal strain textures, with a Meissner-like $e_{1,2} = 0$ expulsion [11]. In coordinate space, with $\hat{r} \cdot \hat{r}' = \cos(\theta - \theta')$, the potential $U(\vec{r} - \vec{r}') \sim \cos 4(\theta - \theta')/|\vec{r} - \vec{r}'|^D$ has sign-variation supporting elastic frustration, with the OP strain at a point receiving conflicting (“ferro/antiferro”) instructions from other surrounding strains. The power-law ($D = 2$) decay arises from $U(\hat{k})$ being scale-free ($|\mathbf{k}|$ -independent) at long wavelengths, rather than from proximity to some critical point.

Our central physical idea is quite simple. Suppose, among (symmetry-broken) rectangular unit cells $\epsilon(\vec{r}) = 1$, that a single unit-cell is made square, $\epsilon(\vec{r}) = 0$. To maintain lattice integrity, the neighboring (and further) unit cells must also deform, with an admixture of non-OP strains. As shown in simulations of a nonlinear-strain model under local external stress, for $A_{1,2} \gg 1$ the large non-OP energy costs can make it profitable to locally summon up the (degenerate) competing structure, in energy-lowering higher elastic multipoles: a process of *adaptive elastic screening* [11]. Thus a charge, acting as a local internal stress, can produce an unusual sign-varying (i.e. textured) extended polaron modulated by the anisotropic $U(\vec{r} - \vec{r}')$, with coupled fields like $m(\vec{r})$ also sign-varying. This *polaronic elasto-magnetic texture*, or ‘*pepton*’ arises from compatibility and competing ground states, and differs from the more familiar magneto-elastic polaron [13] that deforms a single lattice structure.

We now choose parameters. For the martensite *FePd*, physical values [12] can be scaled

[11] to be dimensionless, and $\varepsilon = e_1 = e_2 = 1$ correspond to strains ~ 0.02 ; the scaled stress $p_1 = 1$ (magnetic field $h = 1$) corresponds to ~ 0.02 GPa (~ 0.25 Tesla); and the non-OP and OP elastic constants are $A_1 = 150, A_2 = 300$. We take as illustrative, $A_1 = 50, A_2 = 105, \sqrt{a_0} = 0.5, \sqrt{a_m} = 1, \kappa = 2, T_s = 1, T_{sc} = 0.8, f = 0.3, A_{m1} = +5$, and specific ‘manganite’ (‘cuprate’) model parameter sets as $T_{cm} = 0, A_{nm} = -1, A_{n1} = +5, A_{n\varepsilon} = +2$ ($T_{cm} = 0.6, A_{nm} = +9, A_{n1} = -5, A_{n\varepsilon} = 20$). This is a regime of globally weak magnetism, relatively strong electron-phonon coupling, and dominant compatibility forces.

Simulation of Textures: The free energy $F = F(n, m, \varepsilon)$ minimum is found by the overdamped limit of a general ferroelastic dynamics [11]:

$$\dot{\varepsilon} = -\frac{\partial F}{\partial \varepsilon}; \quad \dot{m} = -\frac{\partial F}{\partial m}. \quad (4)$$

We show selected relaxed profiles [14] of ε, e_1, m , with both \vec{k} and \vec{r} plots needed for a full understanding. Figure 1 shows strain plots in coordinate space (of $e_1(\vec{r})$) and in Fourier space (of $|\varepsilon(\vec{k})|^2$) due to a single charge for ‘manganite’ parameters. The ne_1 local stress term would by itself produce a bare single-sign strain, so adaptive elastic screening is responsible for the observed textured polaron or ‘pemton’. The butterfly-like quadrupolar (and essentially cancelling) lobes of both signs in strain and magnetization, extends over ~ 20 lattice spacings, explicitly illustrating the concept [1, 3, 6] of magnetic and structural [2] ‘nano-scale phase separation’. Bi-pemtons from nearby charges form stripe-like segments.

For increasing random doping at $T = 0.5$, the average magnetization $\langle m \rangle$ rises sharply from zero for $x_e > 0.13$, to e.g., $\langle m \rangle = -0.21$ at $x_e = 0.15$, with symmetry-breaking in the $m(\vec{r})$ carried by the pemtons. Fig. 2 shows the mutually deforming multi-pemtons, forming meandering ribbons of expanded/compressed unit-cell strain $e_1(\vec{r})$ or oriented spins $m(\vec{r})$. Fourier space plots, e.g. of $|\varepsilon(\vec{k})|^2$ (or $|e_1(\vec{k})|^2$), show a four-lobe shape (as in the single-pemton case) reminiscent of diffuse X-ray and neutron scattering [4, 14]. A signature of compatibility forces is the $\vec{k} \rightarrow -\vec{k}$ inversion symmetry (in the squared strain) relating most of the even finescale crinkles. Fig. 2 also shows a reduction, on warming, of both $\langle m \rangle$ and of $m(\vec{r})$ percolation [2, 15], at fixed doping.

Figure 3 shows the effects on the *composite* multipemton of an external spatially varying compressional stress $p_1(\vec{r})$ or magnetic field $h(\vec{r})$, with four quadrants in each picture from the long wavelength modulation. The diagonal plots show the $p_1 \rightarrow e_1, h \rightarrow m$ or direct responses. The off-diagonal plots show the $p_1 \rightarrow m, h \rightarrow e_1$ or *cross* responses, e.g. fine cloud-like gradations reminiscent of STM/TEM pictures [2]; and enhanced magnetic percolation under stress [7]. The CMR/CSR ‘colossal’ effects can be understood through the “compressed \sim magnetic \sim metallic” interconnections, with fields/stresses locally tipping the delicate balance between opposite-sign large values (see vertical scales) of $m(\vec{r}), e_1(\vec{r})$, thus opening up conducting channels both in magnetization (via double exchange), or in compression (via enhanced tunneling). The rich phase diagram [1] of charge- (or pemton-) ordered states could arise from the orienting long-range compatibility forces [16]. Charge profile relaxation into locally compressed regions would describe orbital ordering, or coexisting localized/extended electronic states.

For ‘cuprate’ parameters, the Néel temperature is $T_{cm} = 0.6$, and at $T = 0.5$, the parent compound has a uniform m . Figure 4 shows that a ‘cuprate’ single pemton is smaller, stronger, and sharper than Fig.1. The ‘cuprate’ multi-pemton with $x_h = 0.1$ aligns $\varepsilon(\vec{r})$ into diagonal parallel ribbons, forming bubbles of stripes [3], with changes for higher doping.

In summary, the central insight from our model is that under doping perturbation, a nonlinear lattice can produce ‘intrinsic inhomogeneities’, that are not quenched-defect random

spots, but rather, self-organized annealed-texture responses, induced by the multiscale effects of local lattice-integrity constraints. These *composite* textures vary with T, p_1 or h .

The compatible, *inter*-cell large-strain texturings must be supported by *intra*-cell deformations of the atomic bases (‘microstrain’), reflected in bond angle/length distributions [3,9], and so will be relevant for complex electronic oxides, with atomic bases of tiltable perovskite octahedra (that have directionally bonded transition-metal ions, and polarizable/deformable oxygens [1]). Further electronic structure studies would allow for both electronic and ionic optimizations. Further theoretical work includes exploring parameter space extensively, in 2D and 3D, in overdamped or other [11] regimes; adding charge-hopping dynamics and charge-profile relaxations; and strain-related microscopic modelling e.g. of plane bucklings [17] induced by octahedral tilts. Further experimental work should include STM mapping of symmetry-adapted strains to seek penton signatures.

It is a pleasure to thank Seamus Davis, Carlos Frontera, and Venkat Pai for useful conversations. This work was supported by the U.S. Department of Energy.

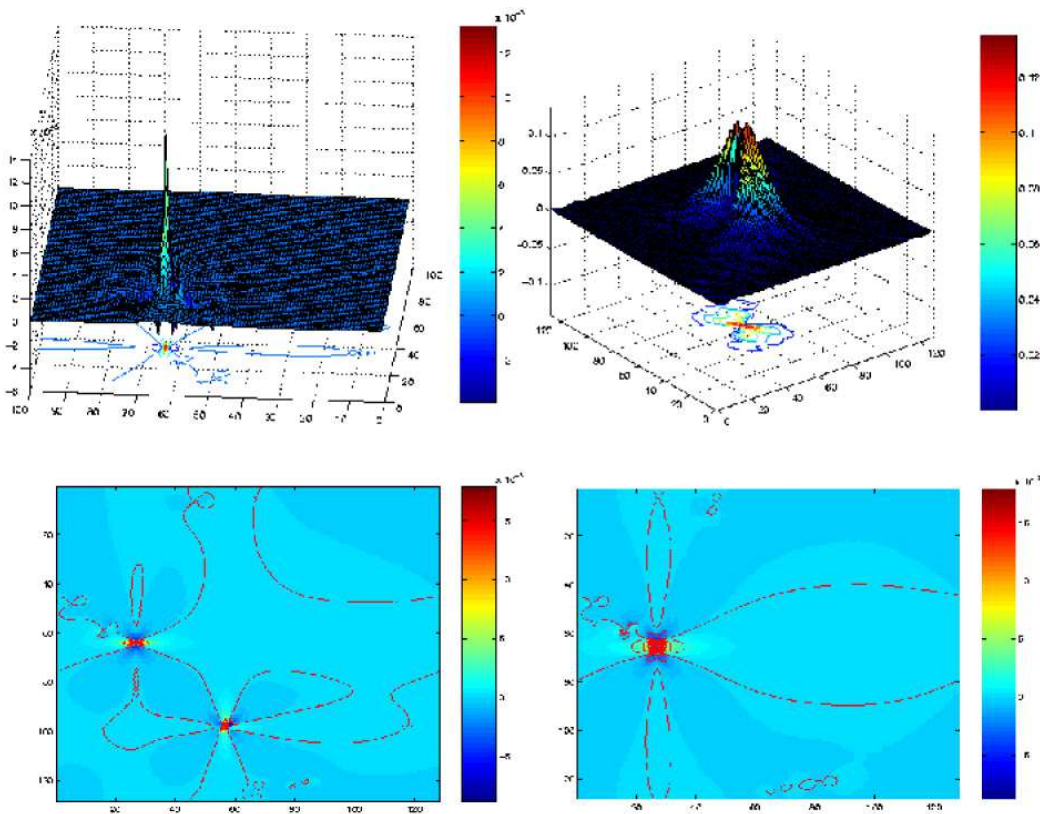


Fig. 1 – Single polaronic elasto-magnetic texture or penton state for ‘manganite’ parameters: Temperature $T = 0.5$. All rows are read left to right. Top row: relief and contour plots of the compressional $e_1(\vec{r})$ strain $\times 10^{-3}$; and Fourier space deviatoric strain of $|\varepsilon(\vec{k})|^2$. Bottom row: colour plot of $e_1(\vec{r})$ for separated and nearby pentons. Note that bi-pentons form stripe segments.

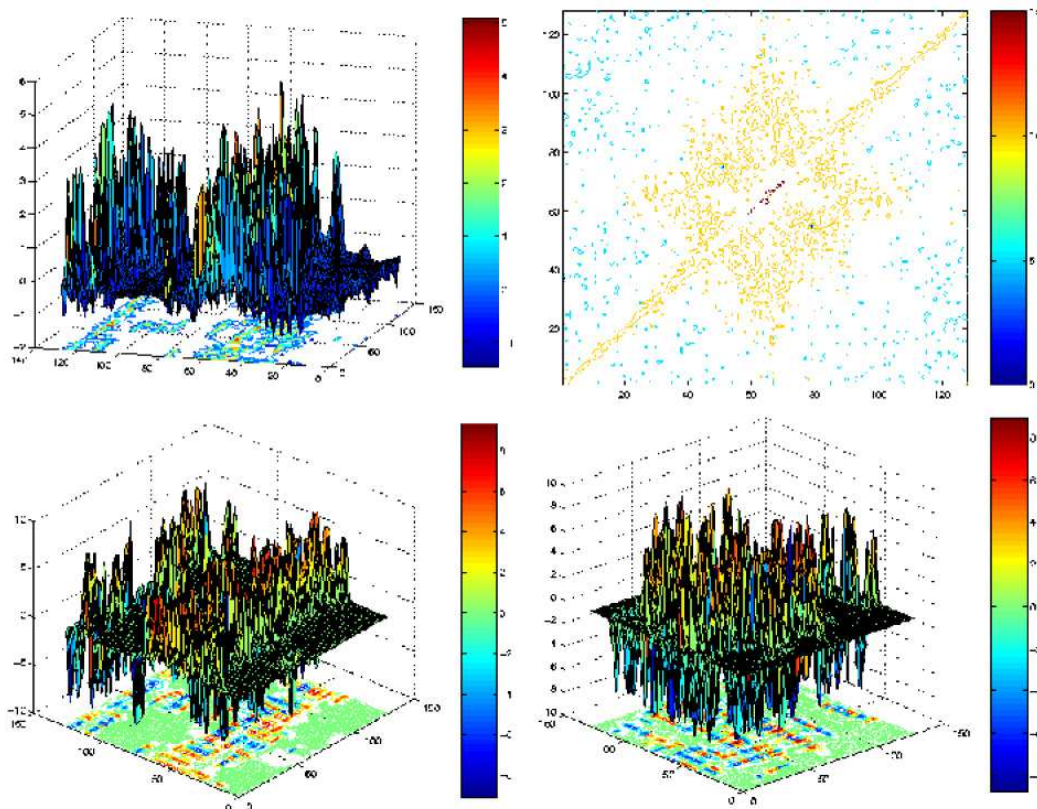


Fig. 2 – Multipempton states for ‘manganite’ parameters: Electron doping fraction $x_e = 0.15$. Relief/contour plots; all rows read left to right. Top row: $T = 0.5$. Plot of the compressional strain $e_1(\vec{r})$. Plot in Fourier space of multiscale $|\varepsilon(\vec{k})|^2$ (log scale). Bottom row: magnetization $m(\vec{r})$ for $T = 0.5$ and 0.8 , with large values compensating to yield $\langle m \rangle = -0.21$ and -0.06 , respectively.

REFERENCES

- [1] *Stripes 2000*, eds. N.L. Saini and A. Bianconi, Int. J. Mod. Phys., **14**, 3289 (2000); *Colossal Magnetoresistance and Related Properties*, eds. B. Raveau and C.N.R. Rao, (World Scientific, Singapore 1998); E.K.H. Salje *Phase Transitions in Ferroelastic and Coelastic Solids*, (Cambridge University Press, Cambridge, UK 1990); N.F. Mott in *Polarons and Bipolarons in High- T_c Superconductors*, ed. E.K.H. Salje, A.S. Alexandrov, and W.Y. Liang, (Cambridge University Press, Cambridge, UK, 1995); A.J. Millis, Nature, **399**, 147 (1998); *Nanoscale Phase Separation and Colossal Magnetoresistance*, ed. E. Dagotto, (Springer, 2003); *Lattice Effects in High- T_c Superconductors*, eds. Y. Bar-yam, T. Egami, J. Mustre-de Leon, and A.R. Bishop, (World Scientific, 1992); *Intrinsic Multiscale Structure and Dynamics in Complex Electronic Oxides*, eds. A.R. Bishop, S.R. Shenoy and S. Sridhar, (World Scientific, 2003).
- [2] M. Faeth, S. Friesen, A.A. Menovsky, Y. Tomioka, J. Aarts, J.A. Mydosh, Science **285**, 1540 (1999); M. Uehara, S. Mori, C.H. Chen, and S-W. Cheong, Nature **399**, 560 (1999); M. Uehara and S-W. Cheong, Europhys. Lett. **52**, 674 (2000).
- [3] A. Bianconi, N.L.Saini, A.Lanzara, M.Messori, T.Rosetti, H.Oyanagi, H.Yamaguchi, K.Oka, and T.Ito, Phys. Rev. Lett. **76**, 3412 (1996); E.S. Bozin, G.H. Kwei, H. Takagi, and S.J.L. Billinge, Phys. Rev. Lett. **84**, 5856 (2000).

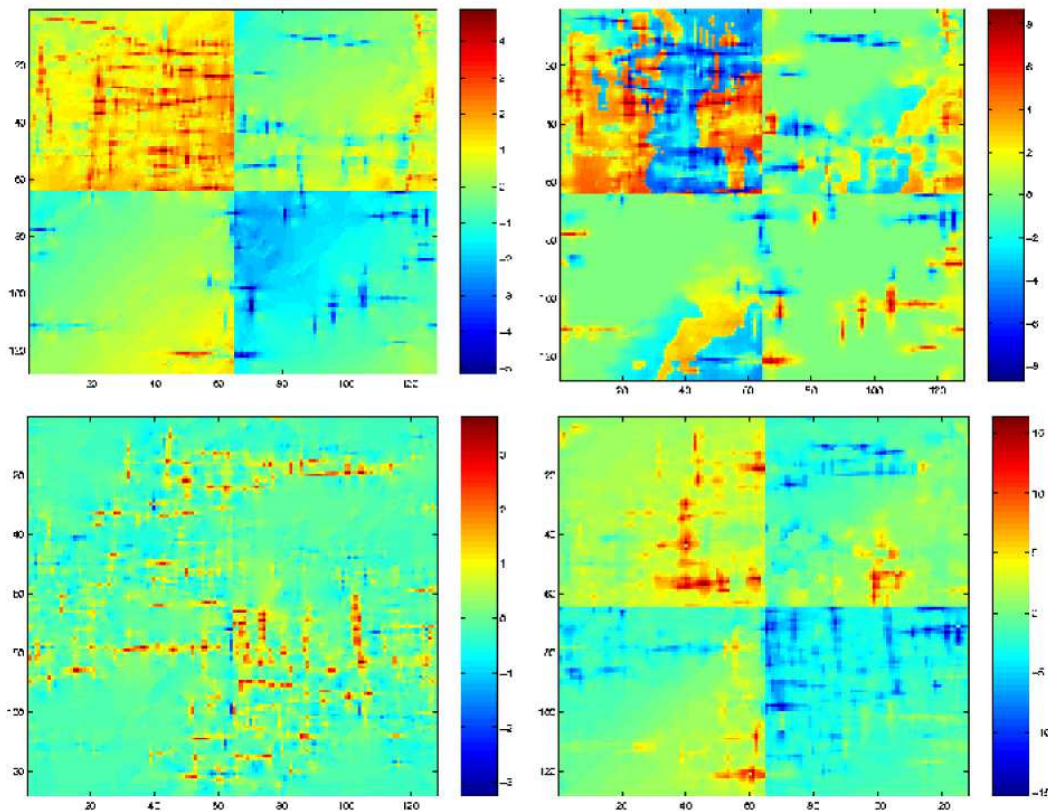


Fig. 3 – Response of ‘manganite’ multi-pemton states to external stress and magnetic field: Doping $x_e = 0.15$, and $T = 0.5$, as in the top left and bottom left of Fig. 2. Colour plots, with all rows read left to right, with four quadrants in each, from the longwavelength variation of stress $p_1(\vec{r}) = p_1 f(\vec{r})$ and magnetic field $h(\vec{r}) = h f(\vec{r})$, where $f(\vec{r}) = \frac{1}{2}[\cos(2\pi x/N) + \cos(2\pi y/N)]$. Top row: $e_1(\vec{r})$ and $m(\vec{r})$ under stress, with $p_1 = 20$ (~ 0.4 GPa). Bottom row: $e_1(\vec{r})$ and $m(\vec{r})$ in a magnetic field, with $h = 10$ (~ 2.5 tesla). Note that $p_1(\vec{r})$ and $h(\vec{r})$ change both e_1 and m , at all scales.

- [4] L. Vasiliu-Doloc, S. Rosenkranz, R. Osborn, S.K. Sinha, J.W. Lynn, J. Mesot, O.H. Seeck, G. Presti, A.J. Fedro, and J.F. Mitchell, Phys. Rev. Lett. **83**, 4393 (1999); S. Shimomura, N. Wakabayashi, H. Kuwahara and Y. Tokura, Phys. Rev. Lett., **83**, 4389 (1999).
- [5] G.-M. Zhao, K. Conder, H. Keller and K.A. Mueller, Nature **381**, 676 (1996); G.-M. Zhao, K.K. Singh, and D.E. Morris, Phys. Rev. B **50**, 4112 (1994); D. Zech, H. Keller, K.A. Mueller, K. Conder, E. Kaldis, E. Liarakapis, and N.Poulakis, Nature **371**, 681 (1994); D. Rubio Temprano, J. Mesot, S. Janssen, K. Conder, A. Furrer, H. Mutka, and K.A. Mueller, Phys. Rev. Lett. **84**, 1990 (2000).
- [6] J. Burgy, M. Mayr, V. Martin-Mayor, A. Moreo and E. Dagotto, Phys. Rev. Lett. **87**, 277202 (2001); M.B. Salamon, P. Lin, and S.H. Chun, Phys. Rev. Lett. **88**, 197203 (2002).
- [7] Y. Hwang, T.M.Palstra, S-W. Cheong, and B. Batlogg, Phys.Rev.B **52**, 15046 (1995); A.N. Lavrov, S. Komiya, and Y. Ando, Nature **418**, 385 (2002). S.B. Ogale, V.Talyansky, C.H.Chen, R.Ramesh, R.L.Greene, and T. Venkatesan, Phys. Rev. Lett. **77**, 1159 (1996).
- [8] J. Zaanen and O. Gunnarson, Phys. Rev. B **40**, 7391 (1989); S.A. Kivelson and V.J. Emery, Physica C **235**, 189 (1999); F. Kusmartsev, Phys. Rev. Lett. **84**, 5026 (2000).
- [9] C. Zener, Phys.Rev.**71**, 846 (1947); J. McAllister, and J.P. Attfield, Phys.Rev.B**66**, 04514 (2002)

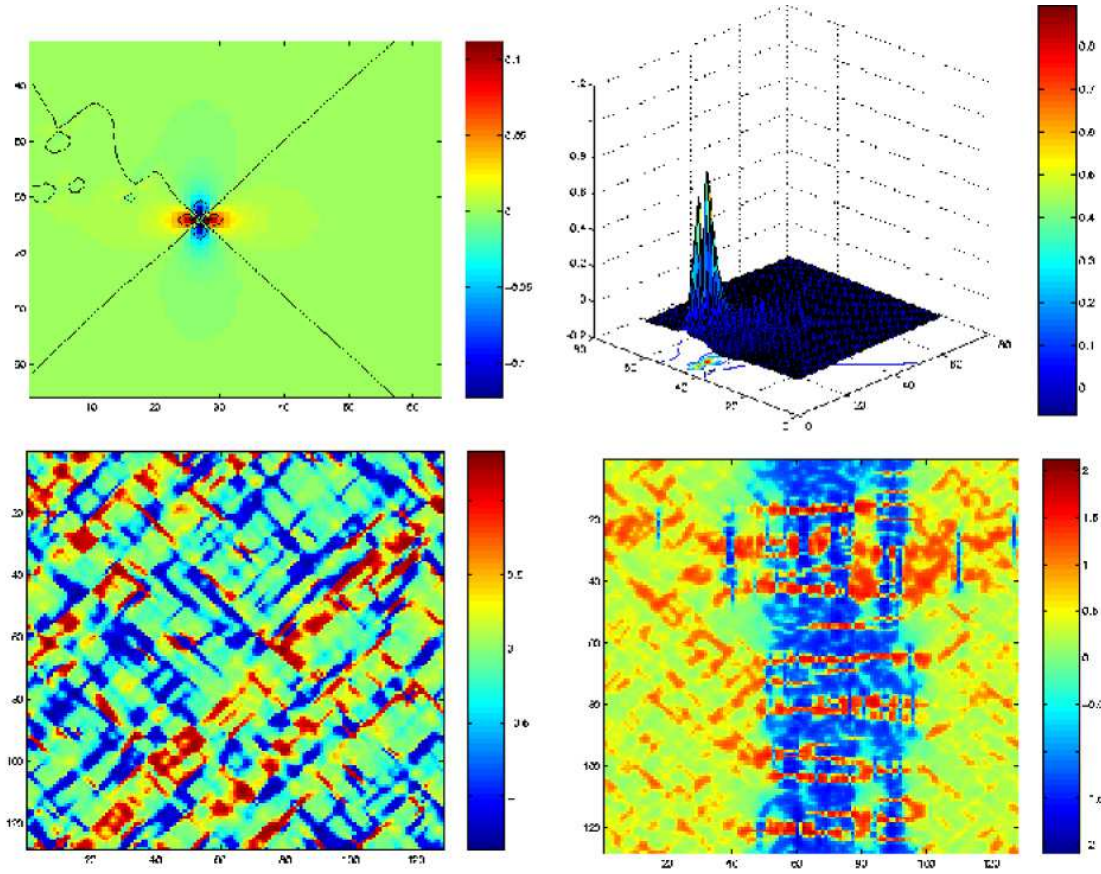


Fig. 4 – *Pemtons* for ‘cuprate’ parameters: Temperature $T = 0.5$; parent compound (subtracted) has Néel temperature $T_{cm} = 0.6$. All rows read left to right. Top row: Colour plot of single-pemton $e_1(\vec{r})$. Relief/contour plot of staggered magnetization $m(\vec{r})$ with $\langle m \rangle = 3 \times 10^{-3}$. Bottom row: Colour plots of $\varepsilon(\vec{r})$ for random pentons with hole fractions $x_h = 0.1$ and 0.2 .

- ; K. Iwano, Phys. Rev. B **64**, 184303 (2001).
- [10] M. Baus and R. Lovett, Phys. Rev. Lett. **65**, 1781 (1990); Phys. Rev. A **44**, 1211 (1991); D.S. Chandrasekharaiyah and L. Debnath, p. 218, *Continuum Mechanics*, (Academic, San Diego, 1994).
- [11] S.R.Shenoy, T.Lookman, A.Saxena, and A.R.Bishop, Phys. Rev. B **60**, R12537 (1999); K.Ø. Rasmussen, T.Lookman, A.Saxena, A.R.Bishop, R.C.Albers, and S.R.Shenoy, Phys. Rev. Lett. **87**, 055704 (2001), T. Lookman, S.R. Shenoy, K. Rasmussen, A.Saxena and A.R. Bishop, Phys. Rev. B **67**, 021301 (2003).
- [12] S.Kartha, J.A. Krumhansl, J.P. Sethna and L. Wickham, Phys. Rev. B **52**, 803 (1995).
- [13] H. Roeder, J. Zhang, and A.R. Bishop, Phys. Rev. Lett. **76**, 1356 (1996).
- [14] We consider 128×128 systems and periodic boundary conditions, with charge profiles introduced through their site Fourier transforms. We first relax the strain by itself, from initial $\varepsilon(\vec{r}, t = 0)$ random within ± 0.2 . The magnetization is then coupled and relaxed from $m(\vec{r}, t = 0)$ fluctuations around the zero-doping meanfield value. This ‘parent compound’ has (unequal-separation) diagonal domain walls, usually with a few metastable kinks. Charges are added at fixed random positions (but forbidding double occupancy). Further relaxations are up to 3×10^4 time steps,

with step size $\Delta t \sim 0.01$, using as equilibration diagnostics, the free energy and its 'force' derivatives, and variable averages and max/min values. The parent background is then subtracted. Signatures of (charge-deformed) background kinks and twins can show up in the Figs.

- [15] On cooling, nonzero (positive and negative) $m(\vec{r})$ 'metallic' regions could possibly percolate across the system at the same insulator-metal transition temperature. Then symmetry-breaking to a nonzero $\langle m \rangle$ between these competing-sign backbones could occur at a lower ferromagnetic temperature. Alternatively, for other parameters, isolated islands could order ($\langle m \rangle \neq 0$) before percolation, inverting the sequence of the transitions.
- [16] In our model, for periodic charge arrays, momentum conservation on the n, m, e_1 couplings of (3) imply that dominant (single) wavevectors are related by $k_n = 2k_m = k_1$.
- [17] S.R.Shenoy, V.Subrahmanyam, and A.R.Bishop, Phys. Rev. Lett., **79**, 4657 (1997); D. Mihailovic, V. Kabanov, and K.A. Müller, Europhys. Lett. **57**, 254 (2002).